Tsai & Hung: High-precision surface metrology system using structured light projection

Wednesday, February 10, 2021 3:38 PM

1-s2.0-S026
32241050...

This paper mostly has to do w/ very high precision measurement. Stopped reading partway thru bc couldn't understand.

Available online at www.sciencedirect.com
SCIENCE DIRECT®
Measurement 38 (2005) 236–247
Measurement
www.elsevier.com/locate/measurement

Development of a high-precision surface metrology system using structured light projection

Ming-June Tsai [a,1], Chuan-Cheng Hung [b,*]

[a] Robotics and Automation Laboratory, Department of Mechanical Engineering, National Cheng-Kung University, 1 University Road, Tainan 70101, Taiwan
[b] Department of Electronic Engineering, Kao Yuan University of Technology, 1821, Chung Shan Rd., Lu Chu Hsiang, Kaohsiung County 821, Taiwan

Received 3 December 2004; accepted 19 July 2005

Type of sensor, no longer used

Abstract

In this paper, we present a high-precision surface metrology system based on structured light projection. Gray code patterns are projected onto the object surface by a DMD projection device and a CCD camera captures the distorted pattern images. For the purpose of precision measurement, a 3D mathematical model is proposed for the system and a calibration process is developed to obtain system parameters. The pattern is encoded with a unique ID and correspondence pairs between the CCD and DMD can be found. The surface profile can be computed by the calibrated model. In order to acquire higher measurement resolution, we propose a correspondence matching method which combines Gray codes encoding and sub-pixel edge detection. With a line-shifting procedure, the measurement resolution is elevated four times higher. Experiment results demonstrate the system has measurement area of 12×9 mm^2, with lateral resolution about 10 μm and vertical resolution about 3 μm.

Keywords: Structured light; Projector calibration; Surface profile measurement; Digital micro-mirrors device (DMD); Sub-pixel edge detection; Line-shifting

1. Introduction

Because of demanding specifications in current manufacturing industry, surface profile measurement with micron-level precision becomes important to supervise the quality of product. Traditionally, coordinate measurement machines

* Corresponding author. Tel.: +886 7 6077002; fax: +886 7 6077000.
E-mail addresses: mjtsai@mail.ncku.edu.tw (M.-J. Tsai), nelson@cc.kyu.edu.tw (C.-C. Hung).
[1] Tel.: +886 6 2757575x62161; fax: +886 6 2376962.

0263-2241/$ - see front matter © 2005 Elsevier Ltd. All rights reserved.
doi:10.1016/j.measurement.2005.07.014

(CMMs) have been used for surface profile measurement. While it is still extensively used in industries limitations such as low speed, high cost and its contact nature prevent its application in metrology that requires fast and soft material measurement. Optical methods, such as interferometry, stereo vision, structured light projection and shape from focus/defocus, have long received extensive attention. Unlike CMM, measurement systems developed from optical principles is non-contact in nature, thus preventing from mechanical wear and surface deformation problem. Owing to mass production and advanced semiconductor technologies, vision components such as CCD camera and DLP (Digital Lighting Processor) projector are available in recent years, enabling development of a vision-based surface metrology system with low cost and high flexibility [1–6]. Furthermore, since CCD has large measurement range, measurement with millions of points within a few seconds can be accomplished.

Usually a structured light projection system is composed of a projector and a camera. The projector projects a predefined fringe patterns onto the object surface whereas the camera captures distorted image on the surface for further processing. Several methods have been investigated to obtain the surface profile by demodulation of distorted fringe pattern. Among these methods, the most famous one is phase shifting, which calculates the phase of each pixel by so-called four stepping algorithm [7–9]. Since there are major assumptions behind the phase shifting method, the application of measurement and its accuracy is limited. The first assumption concerns with the mathematical description of image patterns, a sinusoidal function is assumed to fit the intensity of fringe pattern on the image. However, it is not true as the fringe patterns are not always formed by interference. Liu et al. developed phase-mapping methods to obtain a phase-height relationship by a tedious calibration procedure [10]. The other assumption is to approximate the arrangement of projection–camera pair as a 2D system [4,11]. The assumption greatly reduces the computational complexity and requires carefully setting up the instrument. However, it is not adequate when the instrument is generally set up and a precision measurement is desired. In order to perform measurement with higher precision, some researchers proposed 3D mathematic models [12,13]. However, in their investigations, projector model is simplified such that only extrinsic parameters are considered.

Another surface measurement method for structure-light projection is the line shifting method [14]. Different from the phase shifting method, line shifting projects a sequence of parallel lines onto the object surface. Positions of line centers are found with sub-pixel accuracy. By shifting the line pattern, the surface profile is quantized into smaller divisions and therefore the measurement resolution is elaborated. Similar to phase shifting, line shifting also requires accurate system model for high precision measurement. In this paper, development of a surface metrology system based on structure light projection is introduced. In order to achieve high precision measurement, the arrangement of projector–camera pair is a general 3D model. A multiple-plane calibration process is developed for projector calibration. Line shifting method with sub-pixel edge/center detection is employed to improve the measurement resolution. With the assistance of gray code encoding, correspondence pair is obtained. Finally, experiment results are demonstrated.

Probably not relevant

2. An overview of projector–camera system

Fig. 1 shows the framework of the system setup. In the setup, fringe patterns are projected onto the object surface by a projection device, which is composed of a DMD (Digital Micro-mirror Device) chip, a light source and a projection lens. The pattern to be projected is generated by a program and transferred to the DMD chip controller by a Universal Serial Bus (USB). The controller controls the tilt angle of totally 1024×768 micro-mirrors on DMD chip. In order to generate a single pattern with different intensity levels, a modulation process similar to pulse width modulation (PWM) is employed. Intensity is controlled by changing the switching duration of each DMD pixel. Since Gray code pattern are utilized in our system, pattern with only two intensity levels is generated.

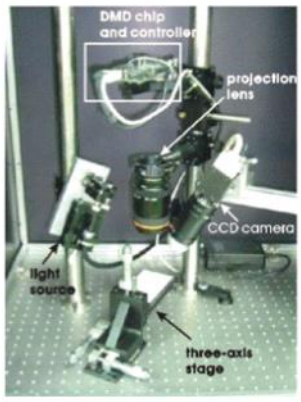

Fig. 1. The developed metrology system.

The pattern on the DMD chip is projected onto the object surface. Object to be measured is placed on the reference plane of a three-axis translational stage. The deformed fringe pattern on the object surface is grabbed by a CCD camera. In order to have larger depth of field (DOF), a telecentric lens is mounted on the CCD. In order to eliminate saturated region resulting from unpolarized light source, linear polarizers are installed in front of CCD lens and projection lens to adjust the polarization state of the light accumulated on the CCD chip.

3. Calibration of projector–camera system

In order to perform measurement, a mathematical relationship between the three-dimensional measurement and the coordinates of both projector and camera must be established. To accomplish this, a precise system model for the projector–camera pair is developed. A calibration process is subsequently performed to obtain parameters of the proposed system model.

For a projector–camera system, parameters can be divided into two groups, namely intrinsic and extrinsic parameters. Intrinsic parameters include image center, effective focal length (EFL) as well as distortion factor, while position of the optical center and orientation of the local coordinate are belong to extrinsic parameters. As mentioned above, some models have been over simplified such that only the extrinsic parameters are considered. If the measured area becomes smaller, its corresponding working distance becomes shorter. Nonlinear effects such as distortion and dislocation of image center become significant. In this section, system model and calibration process are developed in the following sections.

3.1. System modeling

The mathematic model for three-dimensional surface profile computation is shown in Fig. 2. Three coordinate systems are defined as follows: a camera coordinate system (CCS) fixed on the optical center of CCD camera O_C, a projector coordinate system (PCS) fixed on the optical center of the projector O_P, and a world coordinate system (WCS) fixed on the reference plane. During the measurement, fringe pattern to be projected is controlled by each of the micro-mirror on the DMD surface. Suppose ${}^{P}Q_d = [Q_{px} \quad Q_{py} \quad f_P]$ is a pixel locating at the fringe edge on the DMD chip. A pixel ray L_P is formed by projecting ${}^{P}Q_d$ through O_P, and then reaches the surface of the object at ${}^{w}P = [P_{wx} \quad P_{wy} \quad P_{wz}]$. The ray diffracted from a point ${}^{w}P$ on the object surface is captured by CCD sensor and the image is developed at ${}^{c}Q_d = [Q_{cx} \quad Q_{cy} \quad f_c]$ on CCD chip. ${}^{P}Q_d$ and ${}^{c}Q_d$

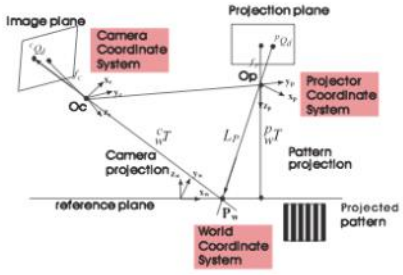

Fig. 2. System model.

forms a correspondence pair which is used to obtain the coordinate of ${}^{w}P$. Therefore, the system can be treated as a stereo camera system, except the projector can only project patterns onto the object. Because of reversibility of a light beam, pixel ray emerges from ${}^{p}Q_d$ and arrive at ${}^{w}P$ is reversible in its direction, and hence ${}^{p}Q_d$ can be considered as the image of ${}^{w}P$ in the DMD array. Consequently, a camera model can be fitted into projector, expressed as follows [15]:

$$\begin{cases} {}^{p}P = {}^{p}_{w}R\,{}^{w}P + {}^{p}_{w}T & \text{(coordinate transformation)} \quad \text{(a)} \\ {}^{p}Q_u = \frac{f_p}{P_{pz}}\,{}^{p}P & \text{(pin-hole projection)} \quad \text{(b)} \\ {}^{p}Q_d(1+\kappa_p r_p^2) = {}^{p}Q_u & \text{(lens distortion)} \quad \text{(c)} \end{cases} \tag{1}$$

where ${}^{p}_{w}R$ and ${}^{p}_{w}T$ are extrinsic parameters which defines the relationship between PCS and WCS, f_p is the effective focal length (EFL), ${}^{p}P = [P_{px} \quad P_{py} \quad P_{pz}]$ is the coordinate of ${}^{w}P$ referred to PCS, κ_p is the distortion factor and $r_p = |{}^{p}Q_d - C_p|$, in which C_p is image center of the DMD chip.

Likewise, CCD camera model is also formulated,

$$\begin{cases} {}^{c}P = {}^{c}_{w}R\,{}^{w}P + {}^{c}_{w}T & \text{(coordinate transformation)} \quad \text{(a)} \\ {}^{c}Q_u = \frac{f_c}{P_{cz}}\,{}^{c}P & \text{(pin-hole projection)} \quad \text{(b)} \\ {}^{c}Q_d(1+\kappa_c r_c^2) = {}^{c}Q_u & \text{(lens distortion)} \quad \text{(c)} \end{cases} \tag{2}$$

Rearranging (1a–c), relationship between ${}^{p}Q_d$ and ${}^{w}P$ is obtained.

$$\begin{bmatrix} r^p_{11}f_p - r^p_{31}Q_{px}h_p & r^p_{12}f_p - r^p_{32}Q_{px}h_p & r^p_{13}f_p - r^p_{33}Q_{px}h_p \\ r^p_{21}f_p - r^p_{31}Q_{py}h_p & r^p_{22}f_p - r^p_{32}Q_{py}h_p & r^p_{23}f_p - r^p_{33}Q_{py}h_p \end{bmatrix} \begin{bmatrix} P_{wx} \\ P_{wy} \\ P_{wz} \end{bmatrix} = \begin{bmatrix} t^p_z Q_{px}h_p - t^p_x f_p \\ t^p_z Q_{py}h_p - t^p_y f_p \end{bmatrix} \tag{3}$$

where r^p_{ij} is each element in ${}^{p}_{w}R$ and $h_p = 1 + \kappa_p r_p^2$, t^p_x, t^p_y and t^p_z are elements of ${}^{p}_{w}T$. Similarly, from (2a–c), relationship between ${}^{c}Q_d$ and ${}^{w}P$ is also derived,

$$\begin{bmatrix} r^c_{11}f_c - r^c_{31}Q_{cx}h_c & r^c_{12}f_c - r^c_{32}Q_{cx}h_c & r^c_{13}f_c - r^c_{33}Q_{cx}h_c \\ r^c_{21}f_c - r^c_{31}Q_{cy}h_c & r^c_{22}f_c - r^c_{32}Q_{cy}h_c & r^c_{23}f_c - r^c_{33}Q_{cy}h_c \end{bmatrix} \begin{bmatrix} P_{wx} \\ P_{wy} \\ P_{wz} \end{bmatrix} = \begin{bmatrix} t^c_z Q_{cx}h_c - t^c_x f_c \\ t^c_z Q_{cy}h_c - t^c_y f_c \end{bmatrix} \tag{4}$$

${}^{w}P$ is determined by applying pseudo-inverse of the matrix formed by the combination of Eqs. (3) and (4). Since Eqs. (3) and (4) involve system parameters including extrinsic and intrinsic parameters of projector and camera, parameter calibration of both devices with high accuracy is very important.

3.2. Calibration process

The calibration process is divided into two steps: CCD camera calibration and projector calibration. Parameters of CCD camera are obtained first. Target points for projector can be generated by projecting patterns on planes with different coordinates. Using information of the CCD camera, coordinates of these target points are calculated.

3.2.1. CCD camera calibration

The objective of calibration process is to obtain the relationship between a group of calibration points referred to WCS and their corresponding images in CCS. A calibration plate (Fig. 3) with 10×10 holes on its top surface is placed on the reference plane. Size and pitch of these holes are machined with very high accuracy and are served as 3D target points during calibration process. The calibration plate is positioned at different height by the X–Y–Z stage, and its image is captured by CCD camera. For each image, geometry center of these holes are calculated, which are considered as image coordinates of target points.

Fig. 4 shows the flow chart for the calibration procedure, which is divided into two steps: linear optimization (Fig. 4a) and non-linear optimization (Fig. 4b). Linear optimization process generates

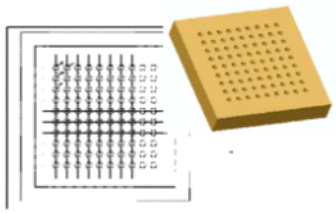

Fig. 3. Calibration plate with 10 × 10 holes.

the parameters R, t, f, κ from given image center (C_x, C_y) and the coordinates of target points that are matched by the correspondence of ${}^{c}Q_d$ and ${}^{w}P$ [16]. In order to evaluate the accuracy of the calibration results, a cost function is defined as $J = \sum_i |{}^{c}Q_d - {}^{c}Q'_d|^2$, where ${}^{c}Q'_d$ is obtained by mapping target points ${}^{w}P$ back to the images using calibrated parameters. The objective of nonlinear optimization is to find the optimal image center (C_x, C_y) by minimizing J with a well-established numerical optimization algorithm [17].

3.2.2. Projector calibration

As for projector calibration, the optimization process is very similar to camera calibration method presented in previous section. The only difference is that the target points are generated by

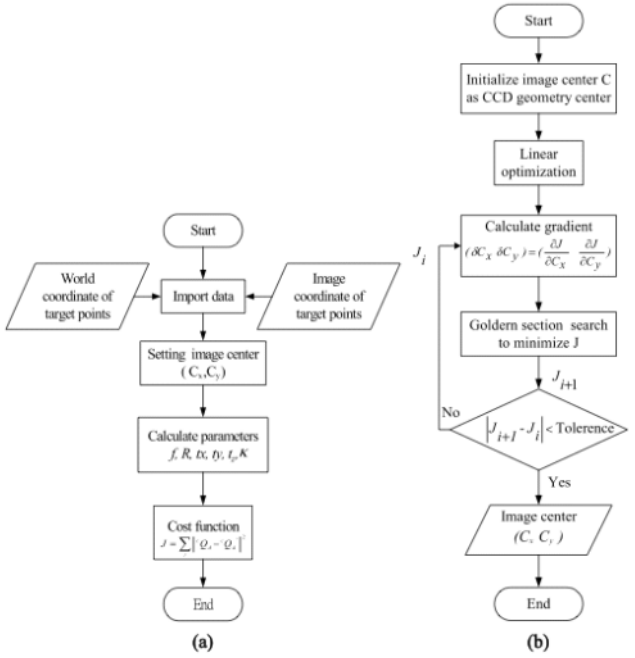

Fig. 4. Calibration process of CCD camera. (a) Linear optimization; (b) non-linear optimization.

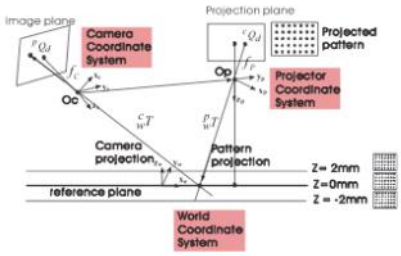

Fig. 5. Generation of non-coplanar targets for projector.

projecting a specified pattern onto planes of different height as shown in Fig. 5. The calibrated CCD camera is used to capture the projected pattern. The x and y-coordinates are calculated by using the camera model. Moving the translation stages at different height produces a group of non-coplanar target points (Fig. 5). The calibration results of both CCD camera and projector are shown in Table 1. It is seen that the image center C_p of the projector is far away from the ideal position (512, 384). The results show that even though the alignment between the DMD chip and the projection lens may not be perfect, the calibration process can still determine the magnitudes of system parameters and compensate the induced error through Eqs. (3) and (4). Fig. 6 shows the residual error of the calibration process. It can be inferred that the accuracy of camera calibration is around 10 μm, while that of projector is around 15 μm.

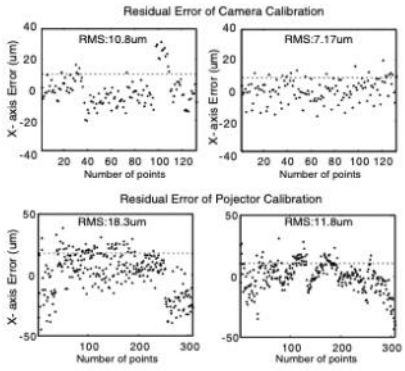

Fig. 6. The residual error of the calibration process.

4. Development of improving accuracy of 3D measurement system

In a structure light projection metrology system, matching correspondence between projection and image sensing device is always an interested research topic. One of the most popular ways is to project fringe pattern onto the object surface, and then using phase calculation, such as four-stepping algorithm, as well as phase unwrapping algorithm to calculate the absolute object phase, which is then converted to surface geometry by a simple relation. In phase-shifting theory, the image intensity is expressed as sinusoidal distribution [18,19],

Table 1
Calibrated parameters of CCD camera and projection device

Parameters	Projection device	CCD camera
Rotation matrix, R	$\begin{bmatrix} -0.99696 & -0.01997 & 0.07530 \\ 0.01537 & -0.97544 & -0.03913 \\ 0.07603 & -0.03877 & 0.99635 \end{bmatrix}$	$\begin{bmatrix} -0.88016 & -0.00834 & -0.47459 \\ 0.00652 & -0.97861 & -0.00879 \\ -0.47449 & -0.01107 & 0.88018 \end{bmatrix}$
Translation vector, T	$\begin{bmatrix} -0.00236 \\ 0.00361 \\ -0.00594 \end{bmatrix}$	$\begin{bmatrix} 0.00592 \\ 0.00183 \\ -0.13753 \end{bmatrix}$
Effective focal length, f (mm)	95.665	192.792
Distortion factor, κ	3.76e−8	1.20e−8
Image center (pixel)	(28.93, 479.42)	(831.0, 420.2)

$$I = I'(x,y) + I''(x,y)\sin[\phi(x,y) + \phi_0] \quad (5)$$

where I' is the background illumination, I'' is the contrast of the fringe image, ϕ_0 is a constant and $\phi(x,y)$ is the object phase. As it has been mentioned above, the illumination background $I'(x,y)$ is assumed to be time-invariant, which is eliminated by four-stepping algorithm. The condition requires a light source with ultimate stability during the phase-shifting process, especially when high precision measurement is desired. Furthermore, in most of the researches the projection and imaging components are arranged on a single plane, leading to a simple relation between object phase $\phi(x,y)$ and surface height. If the phase variation across the measurement area is larger than 2π, a phase-unwrapping algorithm is used to construct the phase map. However, ambiguities occur as the surface has a very large slope change such as a step or a steep groove [20,21].

Correspondence matching provides a robust way for three-dimensional measurement realized by vision components [22–24]. In order to obtain surface measurement with high precision and resolution, correspondence on the projection and imaging planes must be matched perfectly. In this paper, we propose a correspondence matching method which combines Gray code encoding and sub-pixel edge detection. Along with the line-shifting method, the resolution of this system is raised four times higher. Section 4.1 presents the method to encode each fringe with Gray code, and to obtain the positions of the fringe edges and centers with sub-pixel accuracy.

4.1. High precision locating of fringe edges and centers

In order to facilitate correspondence matching, Gray code is used to design the projected pattern such that the measurement area is divided into 256 divisions, with each division having a unique identification code. Using Gray codes as projection pattern has at least two advantages. First, the Gray codes vary exactly in one bit. Thus, it becomes more explicit to solve the spurious decoding problem caused from image noise. Second, the width of each pattern in Gray code pattern is twice as large as that formed by binary code. Therefore, it is indicated that lens with lower modulation transfer function (MTF) can be used with Gray code.

Gray code encoding can only roughly match each division on the projection and imaging devices. To have high precision correspondence, a matching process as shown in Fig. 7 is employed. The matching process can be divided into three steps, namely image processing, edges/centers extraction, and line shifting. Because of the quality of light source and light from the environment, the object is illuminated with uneven intensity and hence limits the contrast of the image, which further increases difficulties in decoding process. Therefore, dynamic threshold is employed to process the original images C_1–C_8 and to eliminate uneven illumination background. The resulting images D_1–D_8 are then quantized into two values, 255 and 0, producing I_1–I_8. Combining I_1–I_8, each pixel on the image is encoded with an identification code. Pixels with the same identification code belong to a single division [25].

In the next step, edges/centers extraction is performed to obtain edges and centers of each fringe. First, position of each fringe edge is obtained using a numerical algorithm. A third order curve is used to fit pixels around the edge, and then secant method is used to zero-crossing position. Since the measurement area has 256 divisions and I_8 has only 128 fringes, positions of fringe centers are also obtained. A center detector algorithm, BR8 [26], is applied to each row of I_8,

$$g_8 = [f(x-4) + f(x-3) + f(x-2) + f(x-1)] - [f(x+1) + f(x+2) + f(x+3) + f(x+4)] \quad (6)$$

where $f(x)$ is the intensity value of position x. As shown in Fig. 8, after process original image with (6), a new image BR8 is produced. The operator as shown in Eq. (6) is a well known Sobel mask, which is a differentiation cascaded by a moving average low pass filter to minimize effects of noise. Therefore, every zero-crossing point in BR8 represents a fringe center in the original image. Likewise, position of each fringe center can be obtained with sub-pixel accuracy by applying the same numerical algorithm to BR8.

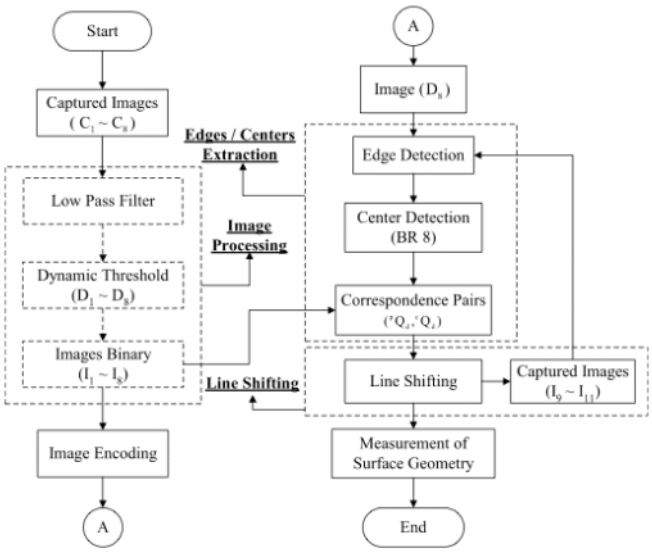

Fig. 7. Correspondence matching process.

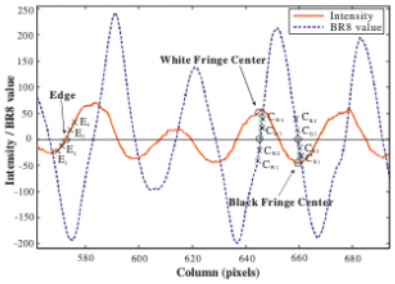

Fig. 8. Edges/centers detection of the fringe patterns.

After the above process, edge position of 256 divisions can be obtained. By matching those edges with ID number generated previously by Gray code decoding process, each edge is uniquely encoded, and correspondence pair $({}^{p}Q_d, {}^{c}Q_d)$ is obtained by matching the encoded edge on both CCD and projector plane. Because the resolution of DMD and CCD chip are different, the projected pattern is scaled by a factor and interpolation is used to correct the difference. With the identified correspondence pair, ${}^{c}Q_d$ and ${}^{p}Q_d$ the three-dimensional information of the point can be computed by Eqs. (3) and (4).

4.2. Combination of edge detection and line-shifting

Since the width of DMD chip has 1024 pixels, for totally 256 fringes there are four pixels wide for each individual fringe. Therefore, the whole measurement area is digitized into 256 divisions horizontally. In order to improve the measurement resolution, the line-shifting technique is employed. In this paper, the line-shifting, as shown

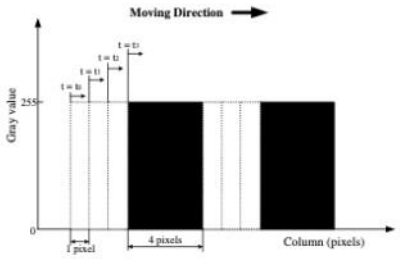

Fig. 9. Line-shifting process of the projected patterns.

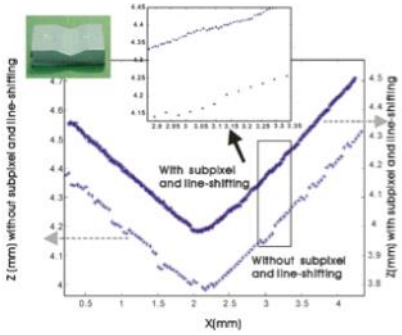

Fig. 10. The measurement results for the V-shape groove.

in Fig. 9, is realized by projecting three more patterns, I_9–I_{11}, onto the object surface. Each fringe pattern is the same as I_8 but has one pixel shifted in the same direction on DMD chip. As a result, the measurement resolution can be elevated up to four times higher than that without the line-shifting.

4.3. Experiment results

Two experiments are demonstrated in this section, one is a V-shape groove while the other is a character on a coin surface. Since the metal surface is highly reflective, the intensities of some regions in the captured image are saturated. As a result, some erroneous codes are generated and give incorrect correspondence pair. In order to have high contrast image patterns, the object surface is coated with a thin layer of white paint. Figs. 10 and 11 show the measurement results for the V-shape groove and the character on the coin, respectively. The groove surface has 1,077,582 data points, spreading over a $12 \times 9\ \text{mm}^2$ area. The edges/centers detection and line shifting method with sub-pixel accuracy is then employed to increase the measurement resolution. The lower part of Fig. 10(a) shows the measurement result without sub-pixel algorithm and line-shifting algorithm. As is expected, the vertical and lateral resolutions are lower. The unsatisfactory result is due to two reasons. First, digital quantization error causes the discontinuities in vertical measurement. Second, since the width of each fringe occupies four pixels, sampling interval across the measurement area is not very small. The upper part demonstrates the result using the sub-pixel algorithm and line-shifting process. The lateral resolution is about 10 μm and vertical resolution is less than 3 μm. In order to evaluate the performance of the system, the sample was also measured by an interferometer based metrology machine, Talyscan-150 (Taylor Hobson Ltd.). As the V-shape groove surface is composed by two inclined planes, the point clouds can be divided into two groups, group #1 and group #2. A fitting process was performed so as to give a quantitative analysis. Each group of points was fitted by a plane $Z = AX + BY + C$. The included angle of two fitted planes is computed. Comparison between the measurement results of two systems is shown in Table 2, in which the difference between two inclined angles is only 2.2%. The time consumed is 2 min, which is only about 2.5% of using Talyscan-150. Additionally, the standard deviations from the fitted plane are also calculated to give an estimation of the measurement resolution.

Another example is a measurement of a coin surface sculpture Fig. 11(a) shows the coin picture and the measurement result of the coin. The character composed by 137,033 data points which cover an area of $3.5 \times 3.5\ \text{mm}^2$ with height of approximately 50 μm, as shown in Fig. 11(b).

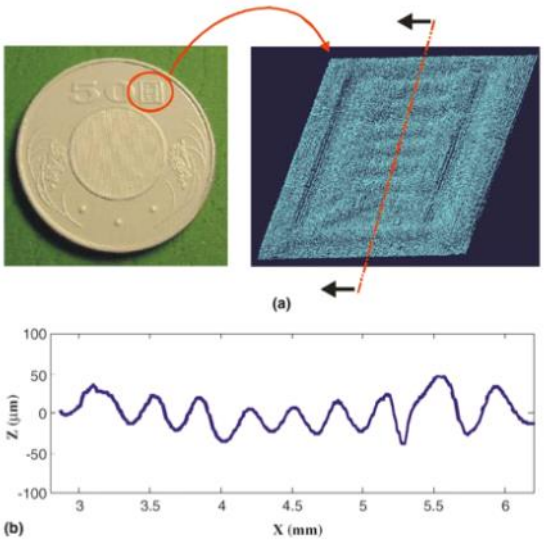

Fig. 11. Correspondence matching process: (a) a real picture and the measurement result of the coin, (b) the cross section of a character on the coin.

Table 2
A comparison between the developed system and Talyscan-150

Measurement results	Developed system	Talyscan-150
Plane equation	$Z_1 = -0.2265X + 0.0016Y + 0.0044$ $Z_2 = 0.2621X + 0.0013Y + 0.0033$	$Z_1 = -0.2159X + 0.0035Y + 0.0014$ $Z_2 = 0.2102X - 0.0018Y - 0.0028$
Standard deviation (μm)	3.817	2.685
Included angle (deg)	152.49	155.92
Measurement area (mm × mm)	12 × 9	16.7 × 2.0
Measurement points	1,077,582	1,321,082
Time consumed (min)	2	90

5. Conclusions and future works

The precision surface metrology system developed in this paper is capable of making full field measurement within a working area $12 \times 9\ mm^2$ without any moving mechanism. The structured light projection is realized by a DMD chip, which makes the generation of projection pattern flexible. Furthermore, the proposed projector–camera calibration method offers a convenient way for general system setup. The experiment results indicate that with Gray code and sub-pixel edges/center

detection, the system is convenient both in setting-up and usage, relative robust, and high precision. Combining line-shifting process, both vertical and lateral resolutions are greatly improved. The two experiments results demonstrate that the developed system has potential for micro-scale precision surface metrology. In the future, if the data registration is implemented to merge measurement data from different locations, the measurement area will be extended without sacrificing the system resolution.

Acknowledgements

This research is being supported by The National Science Council in Taiwan through NSC 92-2623-7-E006-013. In particular we would like to thank Precision Instrument Development Center (PIDC) in Hsinchu for supplying interferometer based metrology machine, Talyscan-150.

References

[1] C. Lu, An absolute depth range measurement of 3-D objects based on modulation Moire topography, in: IEEE International Conference on Pattern Recognition, vol. 1, 2000, pp. 754–757.
[2] M. Fujigaki, Y. Morimoto, Accuracy of real-time shape measurement by phase-shifting grid method using correlation, JSME International Journal, Series A 43 (4) (2000) 314–320.
[3] G. Frankowski, M. Chen, T. Huth, Real-time shape measurement with digital stripe projection by Texas instruments micromirror devices DMDTM, Electronic Imaging Trans. Three Dimensional Image Capture and Analysis III, 2000.
[4] G. Sansoni, M. Carocci, R. Rodella, Calibration and performance evaluation of a 3-D imaging sensor based on the projection of structured light, IEEE Trans. Instrument. Measure. 49 (3) (2000) 628–636.
[5] C.C. Hung, Y.C. Lu, W.H. Yang, A survey on optical 3-D measurement methods for micro-components, in: The Seventh International Conference on Automation Technology, 2003, pp. 77–82.
[6] D. Scharstein, R. Szeliski, High-accuracy stereo depth maps using structured light, in: IEEE Computer Society Conference on Computer Vision and Pattern Recognition, vol. 1, 2003, pp. 195–202.
[7] G. Sansoni, S. Lazzari, S. Peli, F. Docchio, 3D Imager for dimensional gauging of industrial workpieces: state of the art of the development of a robust and versatile system, in: IEEE Proceedings of International Conference on Recent Advances in 3-D Digital and Modeling, 1997, pp. 19–26.
[8] K. Creath, Choosing a phase—measurement algorithm for measurement of a coated LIGO optics, in: Proceedings of SPIE 4101A-06, 2000.
[9] G. Sansoni, 3D Optical whole-field range sensor: development of procedures for the automatic set-up of the measurement and the calibration of the system, in: IEEE Proceedings of Instrumentation and Measurement Technology Conference, vol. 2, 1999, pp. 1154–1159.
[10] H. Liu, B.A. Bard, G. Lu, S. Wu, Absolute measurement of surface profiles with phase-shifting projected fringe profilometry, in: SPIE Proceedings of Optical Manufacturing and Testing III, vol. 3782, 1999, pp. 190–283.
[11] G. Sansoni, L. Biancardi, U. Minoni, F. Docchio, A noval, adaptive system for 3-D optical profilometry using a liquid crystal light projector, IEEE Trans. Instrument. Measure. 43 (4) (1994) 558–566.
[12] S.Y. Chen, Y.F. Li, Self-recalibration of a colour-encoded light system for automated three-dimensional measurement, Measure. Sci. Technol. 14 (2003) 33–40.
[13] C. Sinlapeecheewa, K. Takamasu, 3D profile measurement by color pattern projection and system calibration, in: IEEE ICIT'02, 2002.
[14] J. Gühring, C. Brenner, J. Böhm, D. Fritsch, Data processing and calibration of a cross-pattern stripe projector, in: IAPRS, vol. XXXIII, Amsterdam, 2000.
[15] R.Y. Tsai, A versatile camera calibration technique for high-accuracy 3D machine vision metrology using off-the-shelf TV cameras and lenses, IEEE J. Robot. Automat. RA-3 (4) (1987) 323–344.
[16] T.S. Shen, C.H. Menq, Automatic camera calibration for a multiple-sensor integrated coordinate measurement system, IEEE Trans. Robot. Automat. 17 (4) (2001) 502–507.
[17] W. Press, S. Teuklosky, W. Vetterling, B. Flannery, Numerical Recipes in C++, Cambridge University Press, 2002.
[18] X.Y. Su, L. Xue, Phase unwrapping algorithm based on fringe frequency analysis in Fourier transformation profilometry, Opt. Eng. 40 (2001) 637–643.
[19] O.A. Skydan, M.J. Lalor, D.R. Burton, Technique for phase measurement and surface reconstruction by use of colored structured light, Appl. Opt. 41 (29) (2002) 6104–6117.
[20] D.R. Burton, A.J. Goodall, J.T. Atkinson, M.J. Labor, The use of carrier frequency shifting for the elimination of phase discontinuous in Fourier transform profilometry, Opt. Lasers Eng. 23 (1995) 245–257.
[21] H. Zhau, W. Chen, Y. Tan, Phase-unwrapping algorithm for the measurement of three-dimensional object shapes, Appl. Opt. 33 (1994) 4497–4500.

[22] R.J. Valkenburg, A.M. McIvor, Accurate 3D Measurement Using a Structured Light System, Elsevier Science, 1998, pp. 99–110.
[23] J. Gühring, Dense 3-D surface acquisition by structured light using off-the-shelf components, Report of University of Stuttgart, Germany, 2000.
[24] F. Chen, G.M. Brown, M. Song, Overview of three-dimensional shape measurement using optical methods, Opt. Eng. 39 (1) (2000) 10–22.
[25] M.J. Tsai, C.C. Hung, S.K. Kuo, C.C. Lin, Development of a precision surface metrology system, in: Processing of the 21st National Conference on Mechanical Engineering, 2004, pp. 6505–6511.
[26] R.B. Fisher, D.K. Naidu, A comparison of algorithms for subpixel peak detection, in: J. Sanz (Ed.), Advances in Image Processing, Multimedia and Machine Vision, Springer-Verlag, Heidelberg, 1996.